Available online at www.sciencedirect.com
ScienceDirect
Polymer 49 (2008) 317–329
polymer
www.elsevier.com/locate/polymer

Light scattering from polymer spherulites in crystal growth simulation

Daisuke Tahara*, Yoshihisa Miyamoto

Graduate School of Human and Environmental Studies, Kyoto University, Kyoto 606-8501, Japan

Received 20 August 2007; received in revised form 27 October 2007; accepted 11 November 2007
Available online 17 November 2007

Abstract

A three-dimensional simulation is carried out in the growth process of a polymer spherulite and the Hv light scattering intensity is calculated. In the simulation, a crystallite is represented by a thin disk with the optical axis perpendicular to the disk. In a growth step, each crystallite generates new crystallites, the optical axes of which are fluctuated. The simulation results reproduce prominent features observed in the light scattering experiments on polymer spherulites: the scattering intensity that consists of a fourfold-symmetry intensity component and an isotropic intensity component, the scattering angle dependence, the relative magnitude and the development with crystallization time of these intensity components. A new interpretation is proposed for the Hv light scattering intensity from the polymer spherulites in the growth process.

Keywords: Light scattering; Spherulite; Simulation

1. Introduction

Light scattering gives information on the structure in the scale of the order of μm, and the orientational correlation between the optical elements can be investigated by the polarized light. It has been therefore applied to the analyses of the internal structure of a polymer spherulite.

It is well known that the Hv light scattering from polymer spherulites gives a fourfold-symmetry scattering pattern called a 'four-leaf clover'. The fourfold-symmetry pattern is qualitatively explained by the ideal spherulite model [1]. In addition to the scattering intensity with the fourfold symmetry, the scattering intensity independent of the azimuthal angle μ is observed experimentally and called the isotropic scattering intensity. The method to treat the observed scattering intensity as a sum of these intensities is often referred to Keijzers' combination model [2], and in this model these two intensity components have been independently analyzed. The intensity independent of the azimuthal angle is interpreted to arise from the orientational correlation between the crystallites constituting a spherulite.

On the other hand, several models for the internal structure of a polymer spherulite have been proposed to simultaneously explain these intensities [3–5]. Experimentally the correlation between these intensities is confirmed to exist in the growth process of spherulites [6,7]. Any structure model proposed so far, however, could not satisfactorily reproduce the relative magnitude of these intensities observed experimentally.

In this paper, we perform a three-dimensional simulation in the growth process of a spherulite and calculate the Hv light scattering intensity in order to simultaneously explain the two intensity components and important features characterizing these intensities. We firstly review the experimental results on the Hv light scattering and the related models proposed on the polymer spherulite structure. Then the three-dimension model for simulation is introduced, and the simulation results are compared with the experimental ones in terms of the Hv scattering intensity during the spherulite growth process. Finally, the origin of the isotropic scattering and the development of Hv scattering intensity are discussed.

2. Hv light scattering and spherulite structure models

In this section, the background of this study is set out in more detail. The experimental results on the Hv light

* Corresponding author. Tel.: +81 075 753 6775; fax: +81 075 753 6804.
E-mail address: tahara@z06.mbox.media.kyoto-u.ac.jp (D. Tahara).

0032-3861/$ - see front matter © 2007 Elsevier Ltd. All rights reserved.
doi:10.1016/j.polymer.2007.11.018

scattering of polymer spherulites are often analyzed by Keijzers' combination model [2].

(1) The observed Hv light scattering intensity is composed of the intensity component which has a fourfold symmetry regarding the azimuthal angle, μ, and the one independent of μ. The former is referred to the fourfold-symmetry intensity component $I_{4\text{-fold}}(q,\ \mu) \equiv I(q,\ \mu) - I(q,\ \mu = 0^\circ)$ and the latter, the isotropic intensity component $I_{\text{iso}}(q) \equiv I(q,\ \mu = 0^\circ)$ in this paper, where $I(q,\ \mu)$ is the observed scattering intensity and q is the magnitude of the scattering vector.
(2) The fourfold-symmetry intensity component can be well approximated by the ideal spherulite model [1], which gives an intensity maximum at a polar scattering angle, θ, corresponding q inversely proportional to the radius of spherulite.
(3) The isotropic intensity component decreases with polar scattering angle, and its variation is fitted by the square of the Lorentz function [6,7].

In the ideal spherulite model a volume element in the sphere is uniaxially birefringent with its optic axes in the radial and tangential directions. The Hv scattering intensity from the ideal spherulite, $I_{\text{ideal}}(q,\ \mu)$, is given by [1]

$$I_{\text{ideal}}(q,\mu) = \left(\frac{4\pi}{3}R^3\right)^2 C\mathbf{n}\left[\frac{3\Delta\alpha\cos^2\theta\sin 2\mu}{q^3R^3} \times (qR\cos qR + 3\mathrm{Si}qR - 4\sin qR)\right]^2, \quad (1)$$

where R is the radius of a spherulite, C, a constant, n, the number of spherulites, $\Delta\alpha$, the difference in polarizability between the radial and the tangential directions, and $\mathrm{Si}qR = \int_0^{qR}(\sin x/x)\mathrm{d}x$. Eq. (1) explains the four-leaf clover scattering pattern, but does not give any finite intensity at $\mu = 0^\circ$.

The isotropic intensity component $I_{\text{iso}}(q)$ which is independent of μ, is supposed to originate from the orientation correlation between the crystallites in the spherulites [2,7]. Stein and Wilson presented a general theory of the light scattering from a polymer film possessing randomly correlated oriented fluctuations of optically anisotropic elements [8]. In their approach, a structure is described in terms of correlation functions describing fluctuations in polarizability, magnitude of anisotropy and orientation of the optical axis. Stein and Stidham explained that a random-walk theory results in the exponential correlation function $f(r) = \exp(-r/a)$ for crystals separated by distance r which may fit the correlation functions for many systems [9]. When the spherulite contains crystallites with randomly correlated oriented fluctuations in the orientation and the correlation function is the exponential function with a correlation length much smaller than the radius of spherulite, the isotropic intensity component is given by

$$I_{\text{iso}}^{(0)}(q) = \frac{32\pi^2 C\mathbf{n}\delta^2}{45}\frac{R^3a^3}{\left(1+(aq)^2\right)^2} \quad (2)$$

where a is the correlation length and δ is the anisotropy in polarizability of crystallites. In isotactic polystyrene (iPS), PET and polyethylene, the observed isotropic intensity component has been shown to be expressed by Eq. (2) [6,7,10], and the correlation length a increases with spherulite growth [6,7]. The experimental Hv scattering intensity is thus well interpreted in terms of Keijzers' combination model. Keijzers et al. attributed the fourfold-symmetry intensity component $I_{4\text{-fold}}(q, \mu)$ to the spherulitic crystallites formed at the primary crystallization, and the isotropic intensity component $I_{\text{iso}}(q)$ to the randomly oriented crystallites formed at the secondary crystallization [2]. Mutual interference effects between the two components are not considered.

In a previous light scattering study on the crystallization process of PET [7], however, it has been shown that the optical anisotropy giving the fourfold-symmetry intensity component, $\Delta\alpha$, and the one giving the isotropic intensity component, δ, are proportional to each other, and that the ratio, $\delta/\Delta\alpha$, is almost independent of crystallization time with little dependence on crystallization temperature. The proportional relation has been also shown to exist between the correlation length a determined from $I_{\text{iso}}(q)$ and the spherulite radius R from $I_{4\text{-fold}}(q, \mu)$ [6,7]. These results suggest that these two optical anisotropies, hence two intensity components, originate from the same crystallites with certain arrangements in a spherulite.

In the disordered spherulite model [3,4] the contribution to the isotropic intensity component comes from defective spherulitic structure and is treated as a perturbation from the ideal spherulite. Stein and Chu presented a theory of the light scattering from an anisotropic spherulite with fluctuations in optic axis orientation [3]. Two limiting cases, radial and angular disorders, were considered. Calculations were carried out for various values of the correlation distance characterizing the radial or angular disorder. Increased radial disorder led primarily to increased relative Hv scattered intensity at angles larger than that of the scattering maximum, whereas angular disorder enhanced relative intensity at angles less than the maximum. Yoon and Stein developed a lattice theory of the orientational disorder in two-dimensional spherulites in which the orientation direction of the optic axis in lattice cells is allowed statistically to deviate from its mean value in a manner correlated with the orientation in neighboring cells [5]. Their results are in good agreement with the predictions of Stein and Chu's theory. Since the correlation length a is determined by the local correlation of fluctuation in this model, the increase in a with spherulite growth is left unclarified.

An immature shape of crystal aggregate in the spherulite growth process is proposed as another factor to account for the deviation from the ideal spherulite model [11]. In this fan model, the scattering intensity from a pair of opposing minor sectors is analytically calculated in two dimensions, and the intensity profile is shown to approach that of the ideal spherulite with increasing central angles.

These models depict the important aspects of the deviation from the ideal spherulite, but the considerations have been limited in two dimensions. In the simulation, a condition has been imposed on the crystal aggregate to force the growth in

spherical symmetry, and in the analytical calculations, only simple models can be handled. Since the actual spherulite formation is a result of unlimited growth, the growth of a crystallite aggregate is simulated in three dimensions without invoking a lattice, and the growth process is analyzed including the fanning process.

3. Simulation method

A polymer crystal typically consists of the lamellae formed by the folded chains. The lamellae stack and iterate branching by screw dislocations and overgrowth, so the crystal fans out. After sufficient growth, it becomes a spherical crystal, a spherulite.

In our simulation, the structure unit is a thin disk called a crystallite, which represents a stack of lamellar crystals. Though the lamellar stack contains both amorphous and crystalline regions, and the structure can affect light scattering intensity, we assume that the lamellar stack has uniform optical property for simplicity. The fluctuations in orientation of the growing crystallites are introduced, which give stacking and branching of crystallites. The spatial overlapping of crystallites is prohibited in the simulation, which accounts for the lamellar crystals to stop growing when they collide with each other.

A crystallite is a thin disk with the diameter of unit length. We ascribe two unit vectors **n** and **g** to the disk; **n** is normal to the disk and **g** gives a growth direction. The algorithm of the crystal growth consists of two parts: the generation of new crystallites and the elimination of spatially overlapped crystallites.

The first crystallite, the nucleus, is placed at the origin of Cartesian coordinates with **n** and **g** parallel to the z-axis and x-axis, respectively. At the first step, six new crystallites are generated unit length away from the center of the nucleus on the plane of the nucleus. Their positions are determined by the vector **g** as follows. A vector $\mathbf{g}_1$ is the same as the vector **g**, and vectors $\mathbf{g}_2$, $\mathbf{g}_3$,…, $\mathbf{g}_6$ are given by rotating the vector **g** with increments by 60° in the xy plane (Fig. 1). Each crystallite generated in the direction of vector $\mathbf{g}_i$ ($i = 1,2,\ldots, 6$) has the vectors **n** and **g** equal to **n** and $\mathbf{g}_i$ of the nucleus, respectively. Then each new crystallite is tilted by the Euler angles α, β and γ, where α is random between 0° and 360°, $\beta_t \equiv \beta =$ constant and $\gamma = 0°$ (Fig. 2). Here, the rotation α randomizes the axis of tilting β_t. The vectors **n** and **g** of generated crystallites are tilted by the rotation β_t. The left part of Fig. 3 shows the crystal aggregates at the end of the first step. At the second step, the procedures of crystallite generation and tilting are the same as those at the first step except that no crystallite is generated in the direction of $-\mathbf{g}$. Then five crystallites are generated (Fig. 3). This prohibits the growth in the direction of the parent crystallite. After the second step the same procedure is repeated for crystallites generated at the previous step.

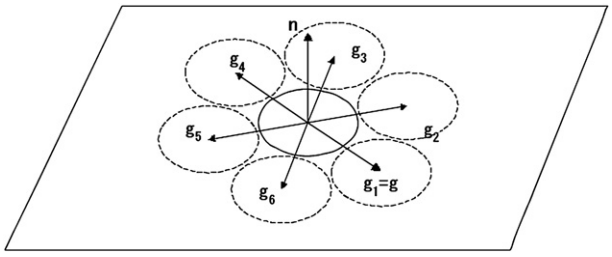

Fig. 1. The nucleus (a solid line) and the crystallites generated at the first growth step (broken lines). The arrows indicate the vectors **n**, $\mathbf{g}_1$, $\mathbf{g}_2$,…, $\mathbf{g}_6$.

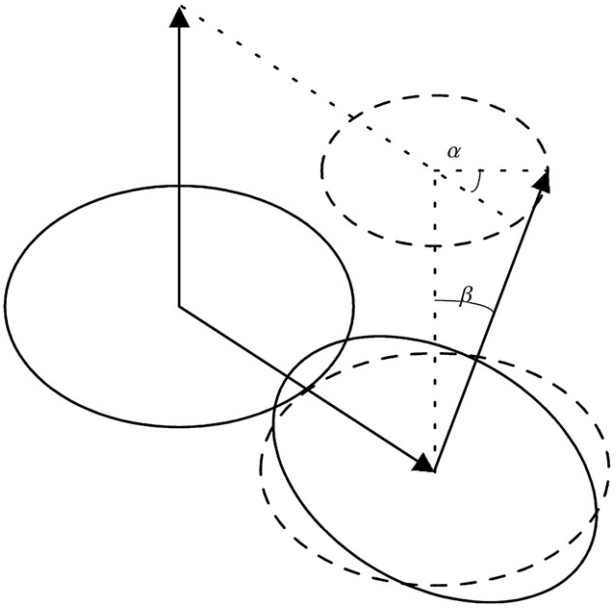

Fig. 2. Tilting of the crystallite by the Euler angles of rotation α and β.

Secondly we describe the elimination process of spatially overlapped crystallites. First a generated crystallite is checked whether it overlaps the crystallites generated at the former steps. If it does, then the crystallite is removed. The crystallite that does not overlap the old crystallites is further checked whether it overlaps the crystallites generated at the same step. When it overlaps another one, one of the two overlapping crystallites is probabilistically removed. A probability of deleting is 0.5 for either crystallites. After checking all the generated crystallites, we fix the crystallites generated at a given growth step.

This algorithm is an extension of the simulation by Yoon and Stein [5]. We expect that the random fluctuations of crystallite orientations give rise to an orientation correlation decaying exponentially, which gives the isotropic intensity component.

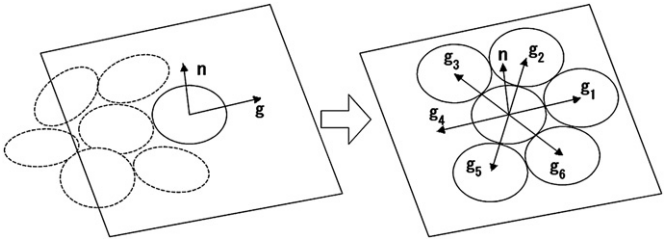

Fig. 3. The crystallites generated at the second step. The left part shows the crystallites after the first step and the plane of a generated crystallite indicated by a square plane. The right part shows the mother crystallite and new crystallites generated at the second growth step.

The intensity distribution in a cross-polarized optical micrograph and the Hv light scattering intensity are calculated as follows. The optical anisotropy of a crystallite is for simplicity assumed uniaxial with a unique axis in the **n** direction and with the magnitude of anisotropy in polarizability of unity. The polarizability of the surroundings must be given in order to calculate the Vv light scattering intensity. We treat therefore only the Hv light scattering in this paper; the calculation of the Vv light scattering intensity will be a future issue. We fix the directions of a polarizer and an analyzer to the x- and y-direction in the laboratory coordinate frame, respectively. The incident light transmits along the z-direction. Given the orientation of a crystal nucleus, we can calculate the light intensity distribution in the real and the reciprocal spaces by rotating the grown spherulite in the laboratory coordinate frame. The orientation of a rotated nucleus, $\mathbf{n}'(\mathbf{r})$, is expressed by

$$\mathbf{n}'(\mathbf{r}) = \widehat{\mathbf{D}}(\alpha,\beta,\gamma)\mathbf{n}\left(\widehat{\mathbf{D}}^{-1}(\alpha,\beta,\gamma)\mathbf{r}\right) \tag{3}$$

where $\mathbf{r}$ is a position vector and $\widehat{\mathbf{D}}(\alpha,\beta,\gamma)$ is the matrix that represents the Euler rotation with the Euler angles α, β and γ.

The intensity at (x, y) of the spherulite image under crossed polars is given by

$$I(x,y) = \left(\int \left(\mathbf{n}'(\mathbf{r})\cdot\widehat{\mathbf{x}}\right)\left(\mathbf{n}'(\mathbf{r})\cdot\widehat{\mathbf{y}}\right)\mathrm{d}z\right)^2, \tag{4}$$

where $\widehat{\mathbf{x}}$ and $\widehat{\mathbf{y}}$ are the unit vectors parallel to the x and y axes, respectively.

The Hv scattering amplitude $F(\mathbf{q})$ of the spherulite is given by the Fourier transformation of $(\mathbf{n}'(\mathbf{r})\cdot\widehat{\mathbf{x}})(\mathbf{n}'(\mathbf{r})\cdot\widehat{\mathbf{y}})$,

$$F(\mathbf{q},\alpha,\beta,\gamma) = \int \left(\mathbf{n}'(\mathbf{r})\cdot\widehat{\mathbf{x}}\right)\left(\mathbf{n}'(\mathbf{r})\cdot\widehat{\mathbf{y}}\right)\exp\left(\mathrm{i}\mathbf{q}\cdot\mathbf{r}\right)\mathrm{d}\mathbf{r}. \tag{5}$$

The scattering amplitude of the spherulite with nucleus oriented the direction determined by α, β and γ is given by Eq. (5) and the scattering intensity, by $|F(\mathbf{q},\alpha,\beta,\gamma)|^2$. At the early steps of the simulation, the spherulite has an immature shape like the one in the fan model. In order to compare the calculated intensity with the experimental results, the scattering intensity is averaged over the orientation of the nucleus. The scattering intensity $I(\mathbf{q})$ is given by

$$I(\mathbf{q}) = \frac{\int |F(\mathbf{q},\alpha,\beta,\gamma)|^2 \sin\beta\,\mathrm{d}\alpha\mathrm{d}\beta\mathrm{d}\gamma}{\int \sin\beta\,\mathrm{d}\alpha\mathrm{d}\beta\mathrm{d}\gamma}. \tag{6}$$

This average corresponds to the situation that the scattering volume contains many spherulites whose orientations are random. The changes of the scattering pattern due to the interference, truncation among spherulites and the distribution of spherulites' size are not taken into account in the present calculation. We assume no distribution of spherulite size in order to compare with the experimental results of PET [7], where the nucleation is approximately instantaneous. We use Rayleigh–Gans–Debye approximation to calculate the scattering amplitude, which is applicable to most polymer spherulites. For highly birefringent systems a more general treatment is necessary [12].

The tilting angle β_t is varied from 5° to 15°. The calculation is carried out for the growth step N up to 70. The number of steps N corresponds to the crystallization time in the experiment and is a measure of the crystal size. When β_t is small, $2N$ approximately equals to the maximum diagonal length of the spherulite.

The experimental results used for the comparison with the simulation results are mainly adopted from a previous study on PET [7], where we have studied the crystallization temperature from 103 to 123 °C. The results at 110 °C shown below are obtained under the same experimental conditions.

4. Results and discussion

The simulation results are compared with the experimental results in the real and reciprocal spaces. Then a new interpretation is proposed for the Hv light scattering intensity from the polymer spherulites in the growth process.

4.1. Real space structure and image

Fig. 4 shows the simulated spherulite and the cross-section through the nucleus at $N = 15$ for $\beta_t = 10°$. The cross-section well reproduces the structure near the spherulite core often observed in the early stage of spherulite formation [13,14].

The effects of the tilting angle β_t on the spherulite structure are discussed first. Fig. 5a and c shows the slices of the spherulite in the x–z plane and the x–y plane for $\beta_t = 10°$ at $N = 20$ and Fig. 5b and d shows those for $\beta_t = 50°$ at $N = 40$. The shapes of the slices in the x–z plane are similar for $\beta_t = 5°$ and 10°. However, the slices in the x–y plane for $\beta_t = 5°$ have more hexagonal shape and the more uniform orientations than for $\beta_t = 10°$. Fig. 5a and c shows the effect of β_t on how

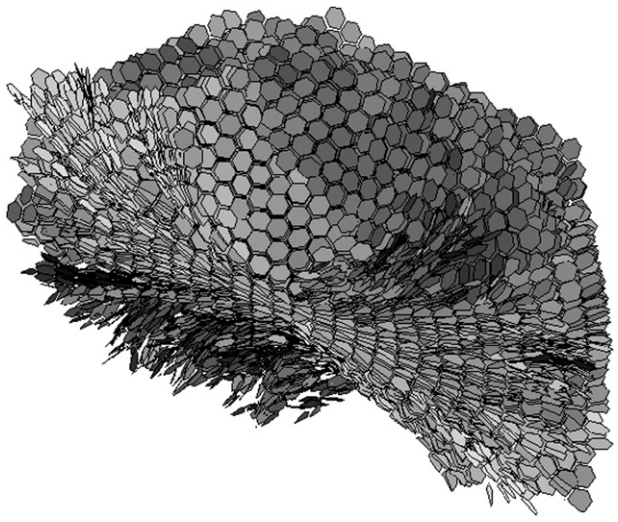

Fig. 4. The simulated spherulite and the cross-section through the nucleus at $N = 15$ for $\beta_t = 10°$.

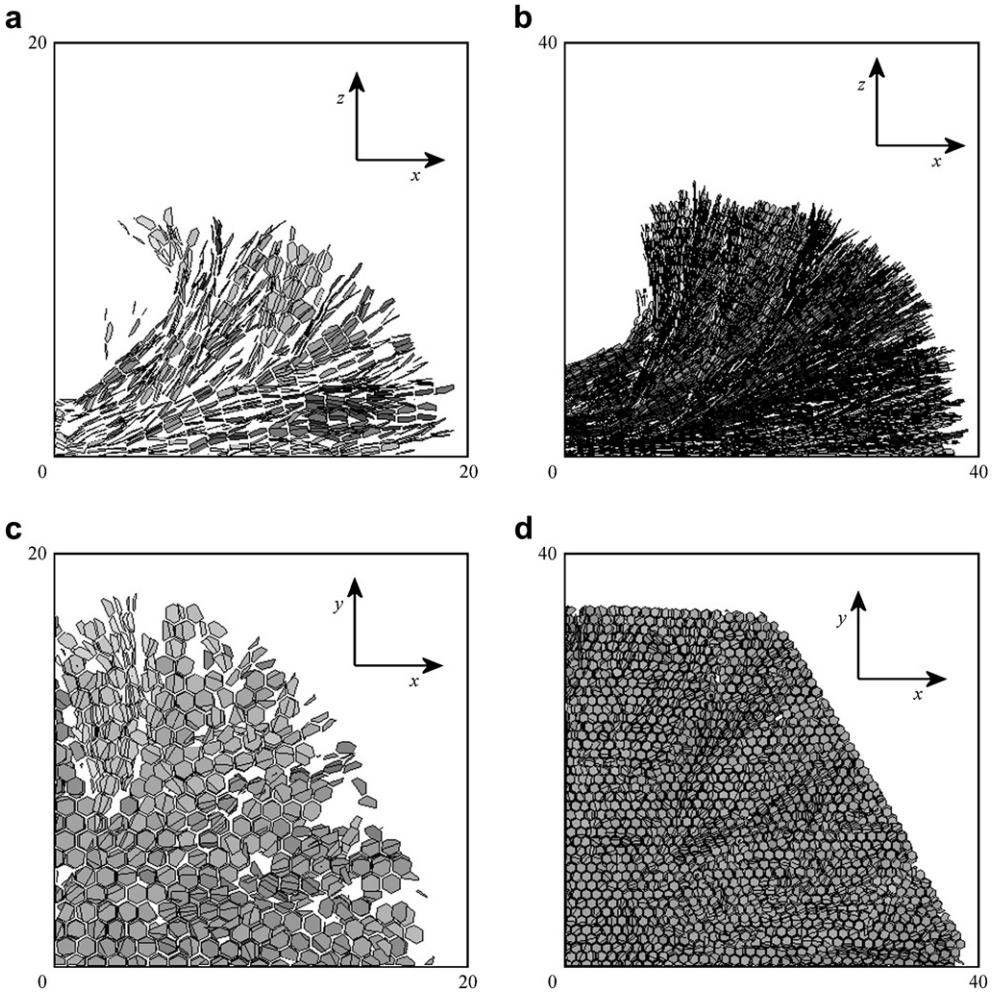

Fig. 5. The slices of the spherulite in the x–z plane (a and b) with thickness 0.5 and the x–y plane (c and d) with thickness 1. The frames are 20×20 for $\beta_t = 10^\circ$ at $N = 20$ (a and c) and 40×40 for $\beta_t = 5^\circ$ at $N = 40$ (b and d).

the spherulite fans out and Fig. 5b and d that on how the orientations of the inner crystallites fluctuate.

The maximum angle φ between the orientation of the nucleus and that of the crystallite at a step N is one of the measures of the degree of fanning in the early stage of the spherulite formation. Fig. 6a shows the growth of φ for different β_ts. The algorithm of the present simulation gives random fluctuation to the orientation of crystallites, while the maximum inclination is approximately proportional to N, since the crystallite that tilts toward free space grows preferentially at the top and bottom surfaces in the z-direction of the spherulite. The slopes of the lines in Fig. 6 are 3.2, 7.1 and 13.2 for $\beta_t = 5^\circ$, 10° and 15°, respectively. The $\beta_t N$ dependence of φ shown in Fig. 6b indicates that the rate of fanning is approximately proportional to β_t.

The orientations of the inner crystallites in the x–y plane fluctuate differently from those at the top and bottom surfaces of the spherulite. In order to examine the orientation fluctuation of the inner crystallites, the orientation correlation between the nucleus and the crystallites at a step N is defined by

$$h(N) = \langle (3\mathbf{n}_0 \cdot \mathbf{n}_N - 1)/2 \rangle, \tag{7}$$

where $\mathbf{n}_0$ and $\mathbf{n}_N$ are the normal vectors of the nucleus and the crystallite generated in the x–y plane and the average is taken over all crystallites generated at a step N lain in $-0.5 < z < 0.5$. Note that the correlation is not taken between all pairs of crystallites but between the nucleus and the crystallites generated at the N-th step in the x–y plane. Fig. 7a shows the change in orientation correlation with N. The correlation lengths obtained by approximating the exponential decay function in the small N range are 264.6, 31.1 and 19.2 for $\beta_t = 5^\circ$, 10° and 15°, respectively. When the collisions among crystallites were not considered, the correlation length would be $2/(3\beta_t^2)$ [9], giving 90.9, 21.9 and 9.7 for $\beta_t = 5^\circ$, 10° and 15°, respectively. When the crystallites collide with each other and some crystallites stop growing, the crystallite whose orientation is different from that of the neighbor crystallites is more likely to stop, and hence the correlation lengths in the simulation are larger than the ones expected from simple random walk. The plots of f to $\beta_t^2 N$ for $\beta_t = 5^\circ$, 10° and 15° approximately fall on a single line (Fig. 7b). This result shows that the correlation length is proportional to $1/\beta_t^2$ in spite of the increase due to the collision.

The results of Figs. 6 and 7 show that the spherulite structure depends on the tilting angle β_t. (i) Change in spherulite

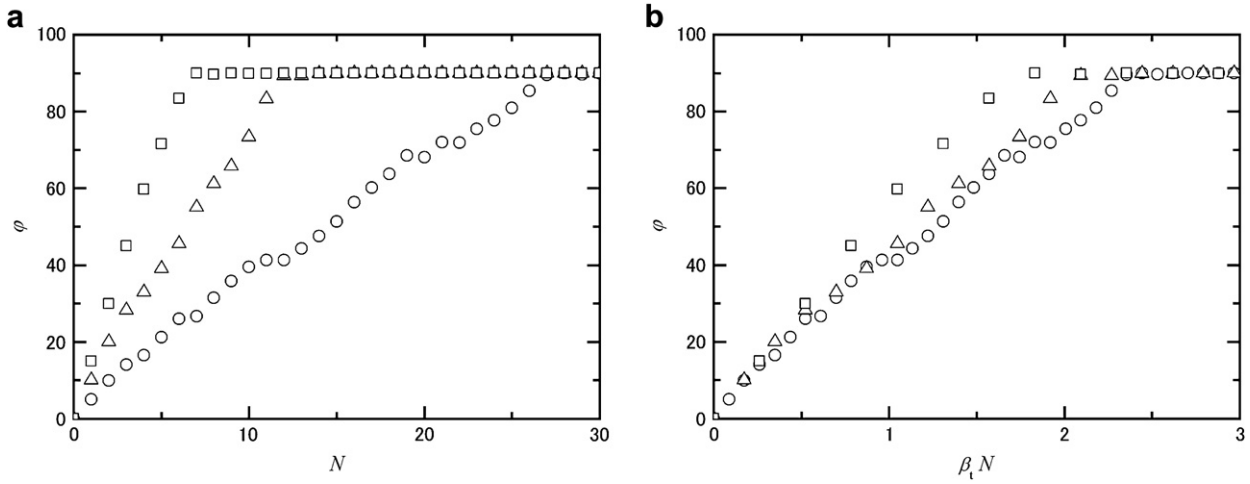

Fig. 6. N dependence (a) and $\beta_t N$ dependence (b) of φ for $\beta_t = 5°$ (circle), 10° (triangle) and 15° (square). Radians instead of degrees are used on the horizontal axis in (b).

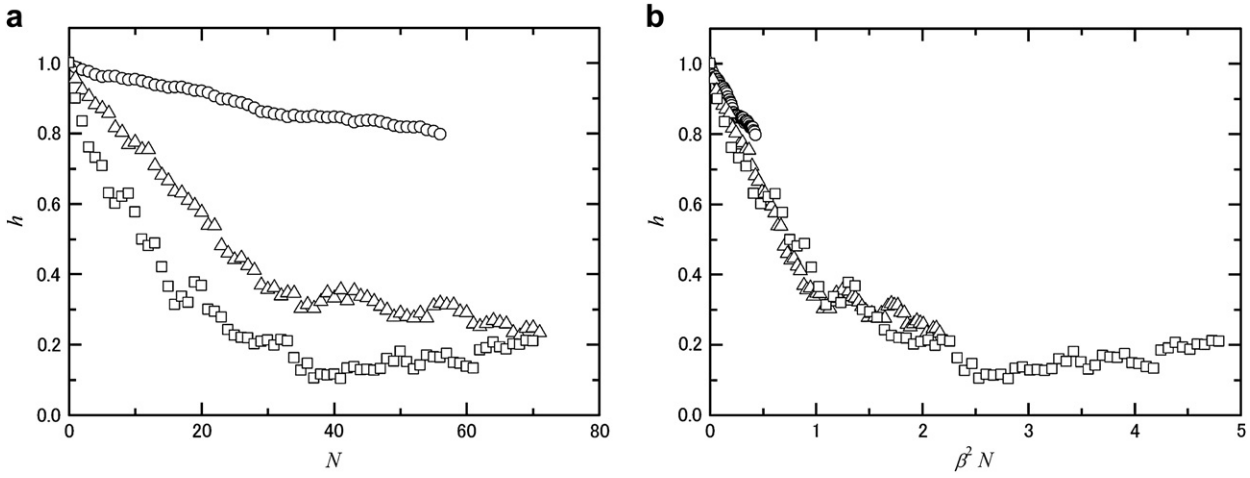

Fig. 7. N dependence (a) and $\beta_t^2 N$ dependence (b) of the orientation correlation f for $\beta_t = 5°$ (circle), 10° (triangle) and 15° (square). Radians instead of degrees are used in (b).

shape approaching to sphere by fanning out is proportional to $\beta_t N$. (ii) On the other hand the memory of nucleus orientation is lost proportionally to $\beta_t^2 N$ in the plane of nucleus. In other words, the valuable $\beta_t N$ is a measure of the shape of the spherulite, while the spherulite of the same size with a smaller β_t has locally the more uniform structure.

In Fig. 7, the increase in orientation correlation is observed at large N. In the early stage of growth, the growth direction crystallite is less restricted and the orientation correlation is expected to decay toward naught ($\langle \mathbf{n}_0 \cdot \mathbf{n}_N \rangle = 1/3$). When the spherulite approaches to a sphere, most crystallites grow in the radial direction on the growth front. In this matured stage of spherulite growth, the orientation of survived crystallites on the circumference in the x–y plane will be random as a whole but locally correlated to escape collision between crystallites. The random orientation correlation around the radial direction leads to $\langle \mathbf{n}_0 \cdot \mathbf{n}_N \rangle = 1/2$, hence $h(N) = 1/4$ as $N \to \infty$. The local correlation in orientation is expected to give a fibrous structure. The growth tip of the slice in x–y plane for $\beta_t = 15°$ and $N = 70$ is shown in Fig. 8. This has fine areas with uniform orientations that correspond the fibrous structure parallel to the radial direction.

The cross-polarized optical micrographs of the simulated spherulites at $N = 20$, 40 and 70 are shown in Fig. 9, illustrating how the spherulite fans out and becomes more spherical with a Maltese cross. The optical micrographs in Fig. 9a–c are calculated by Eq. (4) for the spherulite rotated by the Euler angles (α, β, γ) = (90°, 90°, −90°), and those in Fig. 9d–f, without rotation. Namely, in the former, the direction of **n** and **g** of the nucleus corresponds to the vertical direction and the horizontal direction, respectively, and in the latter, the direction of **n** is perpendicular to the planes of the figures and that of **g** is the horizontal direction.

4.2. Two-dimensional scattering intensity

In this section, the simulation results on Hv light scattering intensity are presented and compared with the experimental results of PET in terms of the fourfold-symmetry component $I_{4\text{-fold}}(q)$ and the isotropic component $I_{\text{iso}}(q)$, and their

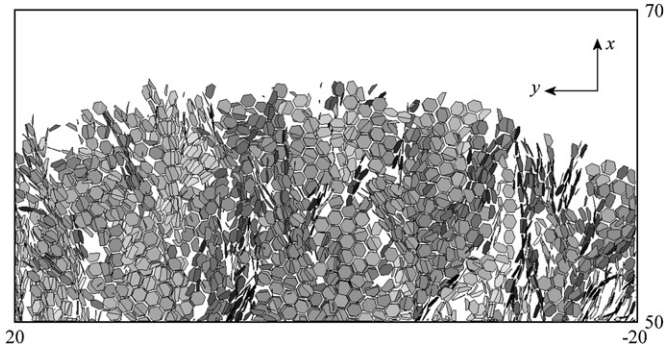

Fig. 8. The edge part of the slice in x–y plane for $\beta_t = 15°$ at $N = 70$ ($50 < x < 70$, $-20 < y < 20$, $-0.5 < z < 0.5$). The direction of x-axis is vertical in this figure.

development with the spherulite growth. Since the spherulite structure depends on the tilting angle β_t as discussed in the previous section, a proper choice of the value β_t may give a better quantitative reproduction of the experimental results. Unfortunately, a value of β_t giving the best fit to the experimental results was not able to be determined among $\beta_t = 5°$, 10° and 15°. In the following discussion, the simulation results will be mainly shown for $\beta_t = 10°$, and comparisons are made with the experimental results.

The two-dimensional patterns of Hv scattering intensity at $N = 10$, 20 and 40 are shown in Fig. 10a–c. These figures show that the diffusive pattern nearly isotropic with regard to μ and decreasing with polar angle θ, becomes the fourfold-symmetry pattern that has peaks against θ, as the spherulite grows. The Hv scattering patterns observed in PET spherulites are shown in Fig. 10d and e: these two experimental data are selected so that the ratios of the isotropic intensity component at $I_{iso}(q = 0)$ to the fourfold-symmetry intensity component at $I_{4\text{-fold}}(q = q_{max}, \mu = 45°)$ agree with those of the simulation results in Fig. 10a and b, where q_{max} is the peak position of the scattering intensity. The scattering pattern corresponding to Fig. 10c was not observed experimentally because the impingements between spherulites prevented spherulites from growing.

The Hv scattering intensity, $I(q, \mu)$, of the polymer spherulites is, as described in Section 1, the sum of the isotropic intensity component independent of the azimuthal angle μ and the fourfold-symmetry intensity component with the μ dependence of $\sin^2 2\mu$. Since the μ dependence of the scattering intensity of the simulated spherulite calculated by Eq. (6) is expressed by Keijzers' model as shown in Fig. 11, we analyze the intensity in terms of Keijzers' model for comparison with the experimental results. The scattering intensity $I(q, \mu)$ is decomposed into the isotropic intensity component, $I_{iso}(q) = I(q, \mu = 0°)$, and the fourfold-symmetry intensity component, $I_{4\text{-fold}}(q, \mu) = I(q, \mu) - I(q, \mu = 0°)$, or $I_{4\text{-fold}}(q) = I(q, \mu = 45°) - I(q, \mu = 0°)$ for brevity.

Fig. 12 shows $I_{iso}(q)$ at $N = 30$. The solid line shows $I_{iso}^{(0)}(q)$ by Eq. (2) with the correlation length $a = 6.78$. The isotropic

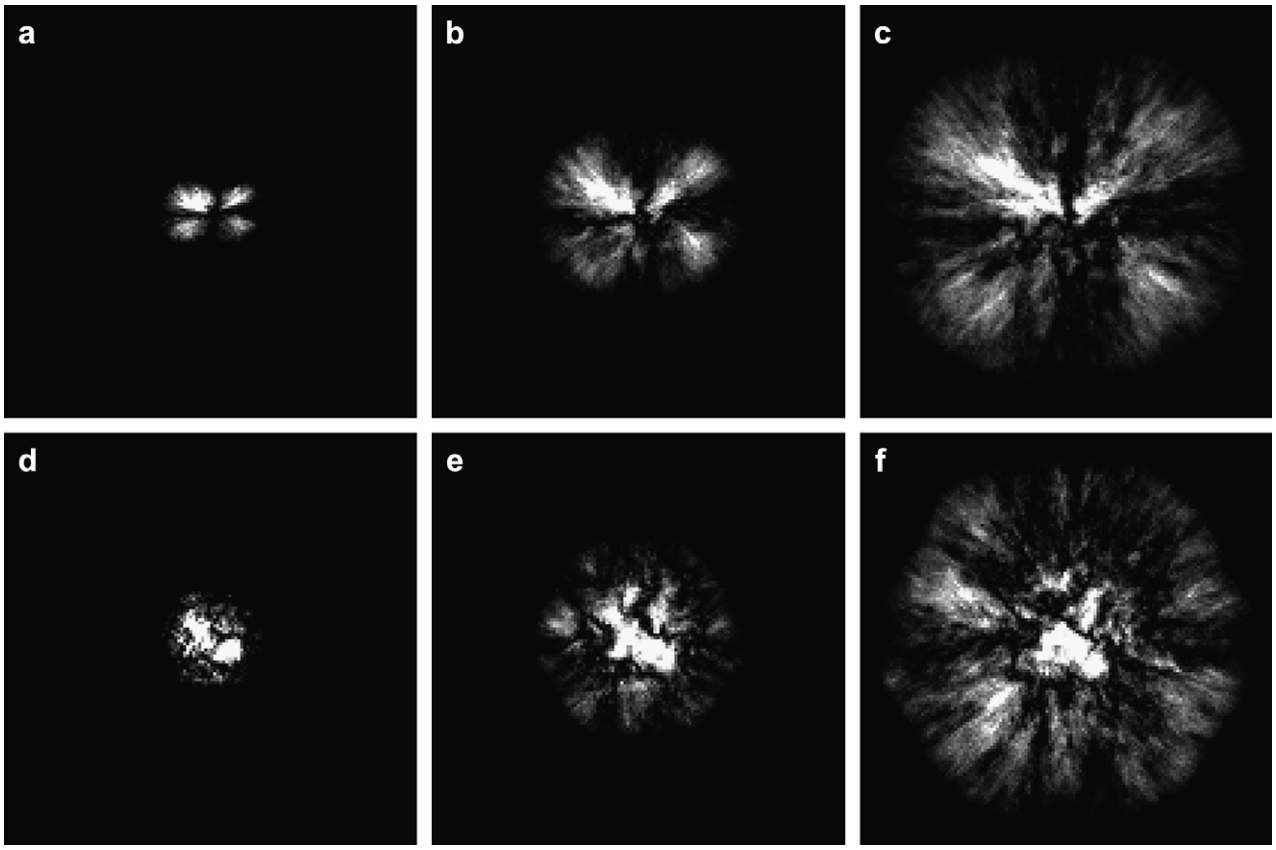

Fig. 9. The cross-polarized optical micrograph image calculated from the simulation at (a and d) $N = 20$, (b and e) $N = 40$ and (c and f) $N = 70$. (a–c) the side views and (d–f) the top views of the spherulite.

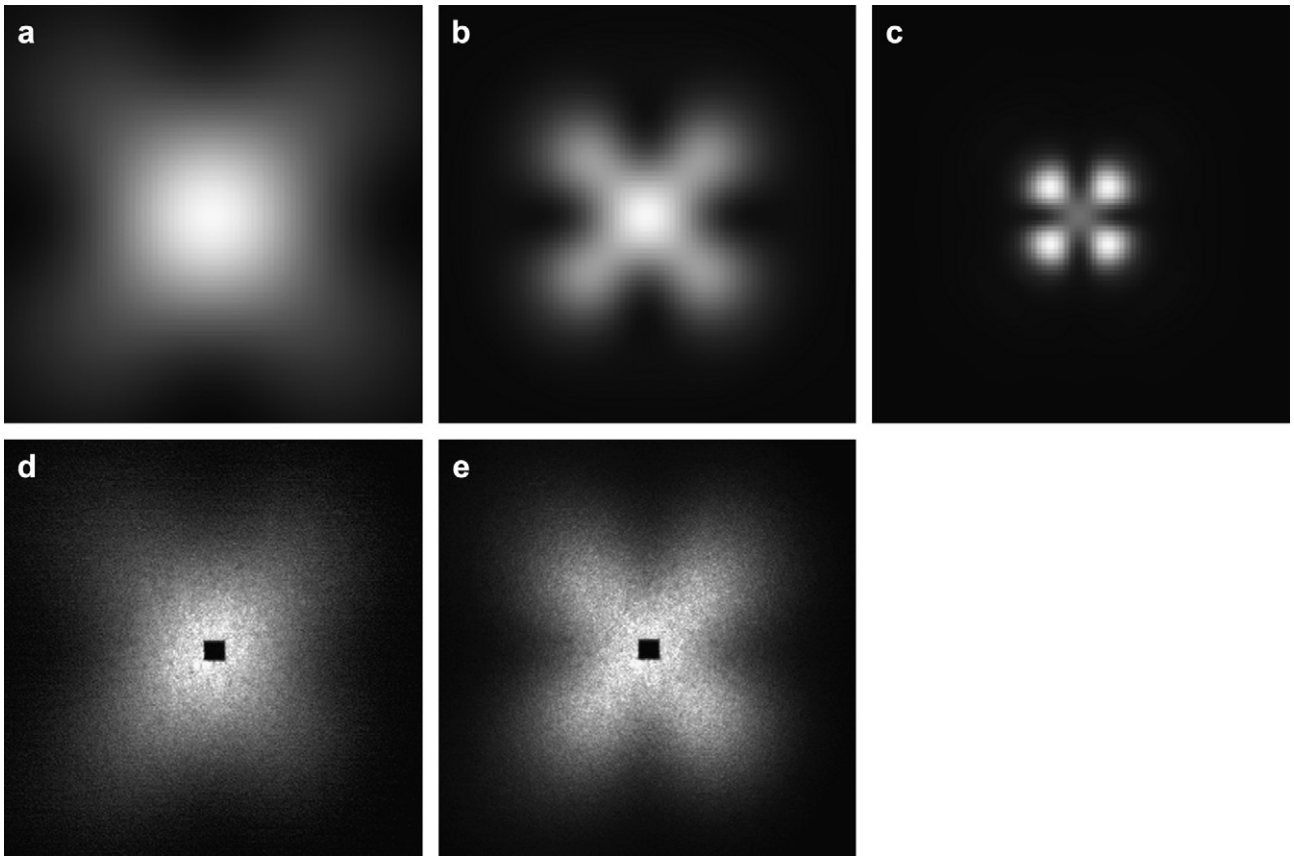

Fig. 10. The Hv scattering patterns from the simulation at (a) $N = 10$, (b) $N = 20$, and (c) $N = 40$. The intensity of each figure is normalized at maximum value: the absolute value of the intensity increases with N. The lower row shows the Hv light scattering patterns from PET spherulites crystallized at 110 °C for (d) 33 min, (e) 66 min. The q at the edge of the figures is 0.613 for a–c and 5.89 μm^{-1} for d and e.

intensity component $I_{iso}(q)$ in the simulation can be well fitted by Eq. (2) in the range $25 < N < 50$ for $\beta_t = 10°$. The spherulite formation process depends on the tilting angle β_t. The number of steps is normalized by $\beta_t^2 N$ as discussed in Section 4.1, and the correlation length by $\beta_t^2 a$. Fig. 13a and b shows the dependence of a on N and that of $\beta_t^2 a$ on $\beta_t^2 N$ for $\beta_t = 5°$, 10° and 15°. The results for various β_t fall on a single line. The normalized correlation length $\beta_t^2 a$ linearly increases with $\beta_t^2 N$ in the early stage of the crystal growth, and stop increasing, when the spherulite becomes large. The approximately linear relation between a and the crystallization time, or the spherulite radius R is observed for iPS [6] and PET [7]. The size of the crystallite disk is estimated to be about 0.1 μm for $\beta_t = 10°$ by comparing the scattering patterns of the PET spherulite to the simulated ones in Fig. 10. The ratio $I_{4\text{-fold}}(q_{max})/I_{iso}(0)$ is used as the measure of the change of the pattern. However, a is 0.54 μm at $N = 20$ for $\beta_t = 10°$ in this simulation (Fig. 10b), whereas a is 0.36 μm in corresponding results in PET spherulites (Fig. 10e). This suggests that a better agreement would be obtained for a larger β_t.

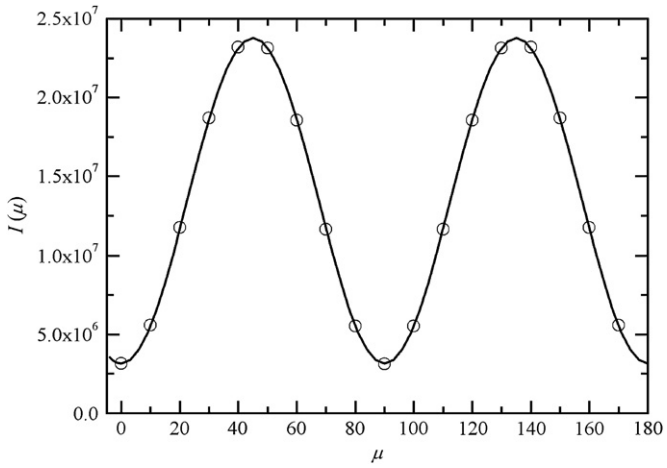

Fig. 11. The azimuthal angle dependence of the scattering intensity in the simulation at q =0.26 and $N = 20$. The solid line shows variation of intensity with μ, $I(\mu) = c_1 + c_2 \sin^2 2\mu$, where c_1 and c_2 are constants.

In Fig. 14, the fourfold-symmetry intensity component normalized by the peak intensity, $I_{4\text{-fold}}(q)/I_{4\text{-fold}}(q_{max})$, is plotted against the normalized scattering vector q/q_{max} at $N = 10$, 30 and 50. The solid line is the result of Eq. (1) for $I_{ideal}(q, \mu = 45°)$. Though the ideal spherulite model explains the profile of $I_{4\text{-fold}}(q)$ of the simulation results, the deviation from $I_{ideal}(q, \mu = 45°)$ is observed at large q, and decreases with increasing N. Similar deviation is also observed in the experiment [7,10]. The cross-term of the fourfold-symmetry intensity component and the isotropic intensity component in

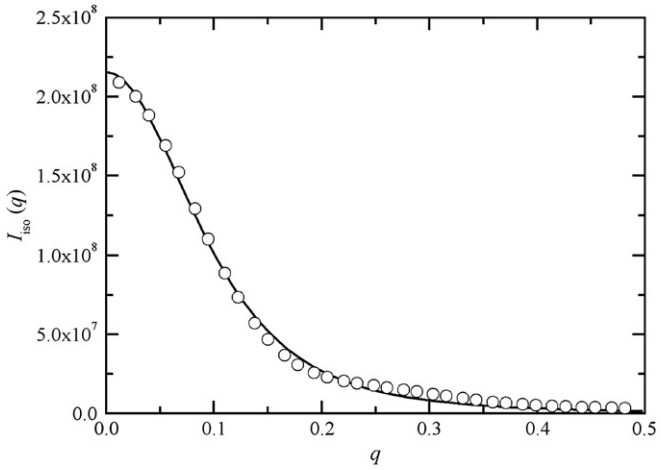

Fig. 12. The q dependence of the isotropic intensity component at $N = 30$. The solid line shows $I_{iso}^{(0)}(q)$ calculated by Eq. (2) with $a = 6.78$.

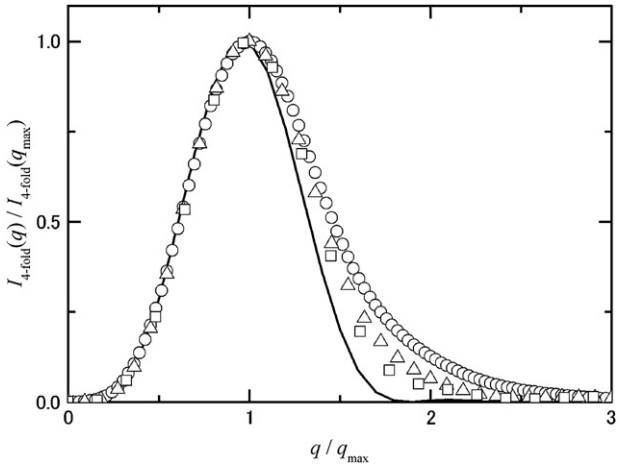

Fig. 14. The q dependence of the fourfold-symmetry intensity component at $N = 10$ (circle), 30 (triangle) and 50 (square) normalized by the peak position and the peak intensity. The solid line shows $I_{ideal}(q, \mu = 45°)$ calculated by Eq. (1) with $R = 4.09/q_{max}$.

the scattering amplitude [10], or the size distribution of spherulites [7] is suggested as the origin of the discrepancy. Since no size distribution is introduced in the simulation, the size distribution may account for only a part of the discrepancy observed experimentally. We will discuss about the change in the scattering profile shortly. The N dependence of the $1/q_{max}$ is shown in Fig. 15. This figure shows $1/q_{max}$ is approximately proportional to N in the simulation, and we obtain the relation $q_{max}N = 4.75$. The "spherulite radius" R is defined by $4.09/q_{max}$ following the convention based on the ideal spherulite model.

According to the disordered spherulite model, the optical anisotropy giving rise to the fourfold-symmetry intensity component is the difference between the tangential and the radial polarizabilities, $\Delta\alpha$, in Eq. (1), and that to the isotropic intensity component, the anisotropy δ in Eq. (2). Since $I_{ideal}(q_{max}, \mu = 45°)$ is proportional to $Cn(\Delta\alpha)^2R^6$ by Eq. (1) with $\cos\theta \cong 1$, and $I_{iso}^{(0)}(q = 0)$, to $Cn\delta^2R^3a^3$ by Eq. (2), $\sqrt{0.178 \times (I_{iso}(0)R^3)/(I_{4\text{-fold}}(q_{max})a^3)}$ from the simulation is a measure of the anisotropy ratio $|\delta/\Delta\alpha|$. The numerical factor

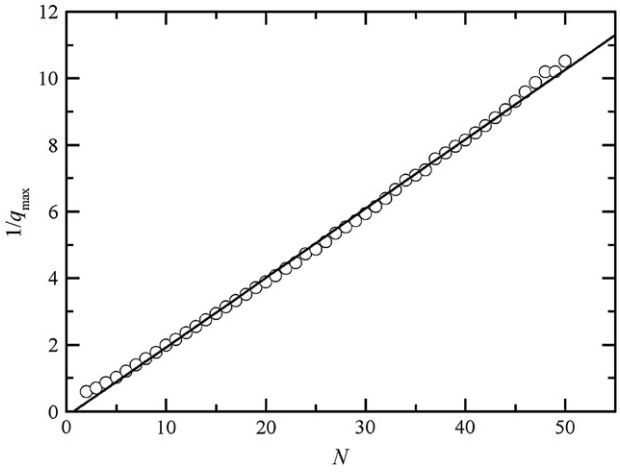

Fig. 15. The N dependence of $1/q_{max}$.

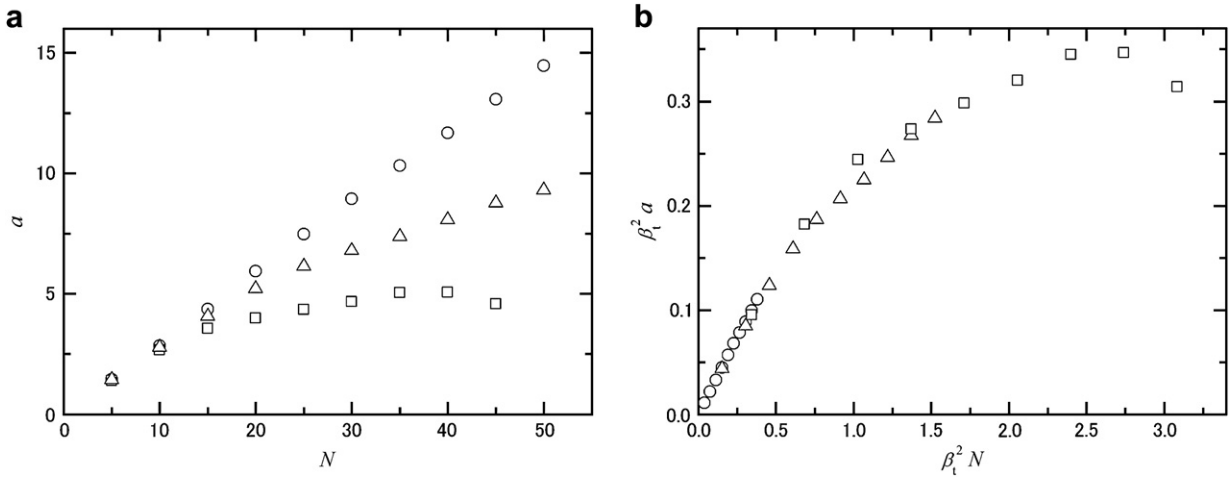

Fig. 13. N dependence of a (a) and $\beta_t^2 N$ dependence of $\beta_t^2 a$ (b) for $\beta_t = 5°$ (circle), 10° (triangle) and 15° (square). Radians instead of degrees are used in the figure.

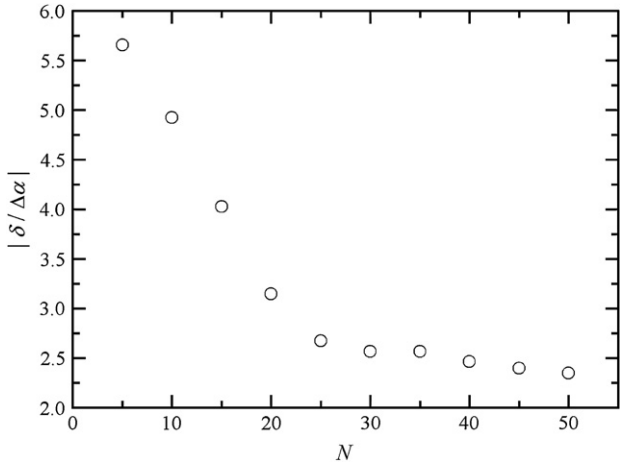

Fig. 16. The N dependence of the anisotropy ratio $|\delta/\Delta\alpha|$.

0.178 is $I_{\mathrm{ideal}}(q = q_{\max}, \mu = 45^\circ)/I^{(0)}_{iso}(q = 0)$. Fig. 16 shows the N dependence of $\sqrt{0.178 \times (I_{iso}(0)R^3)/(I_{4\text{-fold}}(q_{\max})a^3)}$. The anisotropy ratio approaches a constant, about 2, when the spherulite becomes large, while in the experiment it is nearly constant, 4 [7]. Note that the numerical factor is modified to 0.110 instead of 0.178, in a previous paper [7] where the size distribution of the spherulites is taken into account.

The present simulation reproduces the characteristic features of the Hv light scattering of polymer spherulites observed experimentally: (1) the decomposition of the total scattering intensity into the isotropic intensity component $I_{\mathrm{iso}}(q)$ and the fourfold-symmetry intensity component $I_{4\text{-fold}}(q, \mu)$ by Keijzers' model (Fig. 11), (2) the approximation of $I_{\mathrm{iso}}(q)$ by Eq. (2), and $I_{\mathrm{ideal}}(q, \mu)$ by Eq. (1), (Figs. 12 and 14), (3) the correlation between correlation length a and the spherulite radius R or N (Figs. 13 and 15) and (4) the correlation between $I_{\mathrm{iso}}(q)$ and $I_{\mathrm{ideal}}(q, \mu)$ through the optical anisotropies δ and $\Delta\alpha$ (Fig. 16). Based on the agreement between the simulation and the experimental results, we further examine the simulation results, and will discuss about the interpretation of $I_{\mathrm{iso}}(q)$ and $I_{4\text{-fold}}(q, \mu)$ in the growth process of the spherulite.

4.3. Effects of non-spherical shape and origin of isotropic scattering

Some simulation results suggest an interpretation different from the disordered spherulite model for the origins of the two intensity components. The fourfold-symmetry intensity component and the isotropic intensity component are ascribed, respectively, to the ideal spherulitic structure and a perturbation from it in the disordered spherulite model. It is assumed in the model that one spherulite gives these scattering intensities. A spherulite in the simulation is anisotropic due to the orientation of the nucleus. Fig. 17 shows the scattering patterns from a spherulite whose nucleus has a particular orientation. This figure shows the anisotropic pattern although the scattering pattern averaged over the nucleus orientation has the fourfold symmetry (Fig. 10). The fourfold-symmetry intensity component $I_{4\text{-fold}}(q, \mu)$ can be approximated to the scattering from the ideal spherulite model (Eq. (1)) when we separate the total scattering intensity $I(q, \mu)$ according to Keijzers' model, but the spherulite has not become spherical (Fig. 9). As proved in Appendix, the spherulite with the axisymmetric distribution of polarizability in general gives the scattering intensity of Keijzers' model by averaging over the orientation of the nucleus.

We propose a new interpretation for the development of the Hv light scattering intensity, which is analogous to the fan model [11], as follows. (i) In the early stage of the crystal growth, the spherulite is made up of the crystallites with relatively uniform orientation (the central part of Fig. 4). The spherulite is approximated by a circular or hexagonal disk with uniform polarizability, growing with crystallization time. One spherulite gives the anisotropic Hv scattering intensity (Fig. 17b), and the intensity averaged over the orientation mainly consists of the isotropic intensity component (Fig. 10a). Even when the uniform part is small thin disk, the intensity $I(q, \mu)$ is μ dependent, so far as the shape of this part is not spherical (Appendix). The difference in intensity $I(q, \mu) - I(q, \mu = 0^\circ)$ is therefore meaningless as a "spherulite" scattering in this stage. (ii) In the fanning stage,

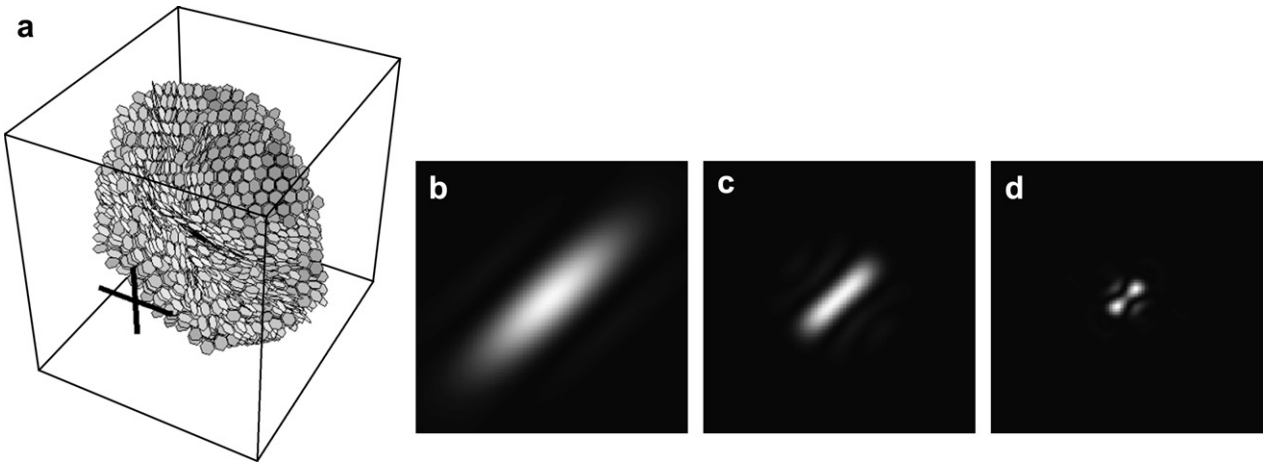

Fig. 17. The scattering intensity patterns from a spherulite oriented in a particular direction shown in (a), (b) $N = 10$, (c) $N = 20$ and (d) $N = 40$. The cross-lines in (a) indicate the directions of the polarizer and the analyzer.

the crystallites with more or less spherical symmetry grow around the central part with uniform polarizability which may be still growing, and the spherulite approaches spherical in shape (Fig. 9a, b and d, e). The scattering from single spherulite is still anisotropic (Fig. 17c and d), and the orientation averaged intensity $I(q, \mu)$ consists of both components $I_{iso}(q)$ and $I_{4\text{-fold}}(q, \mu)$ (Fig. 10b and c). Both the central part with uniform polarizability and the spherically symmetric parts give contribution to $I_{iso}(q)$ with a main contribution from the former, and $I_{4\text{-fold}}(q, \mu)$ with a main contribution from the latter. As the spherulite grows, the volume fraction of the central uniform part decreases. Then $I_{4\text{-fold}}(q, \mu)$ dominates over $I_{iso}(q)$ and is better described by the ideal spherulite model, Eq. (1), with the growth of the spherulite as shown in Fig. 14. (iii) In the matured stage, only the spherically symmetric parts grow and the spherulite becomes fully spherical, mainly giving the $I_{4\text{-fold}}(q, \mu)$. Note that the effects of the fluctuation in orientation in a short distance and of the size distribution are completely neglected in the present discussion. In the present study, the development from stage (i) to (ii) is supposed to be simulated. In a still more rough description, the uniform circular disk grows in the initial stage. The intensity $I(q, \mu)$ is given by the scattering from the uniform disk. Then, the spherically symmetric parts start growing on the uniform disk, giving $I_{4\text{-fold}}(q, \mu)$, and at the same time the uniform disk giving $I_{iso}(q)$ stops growing. In the final stage, spherulite increases the diameter, and $I(q, \mu)$ is given by $I_{ideal}(q, \mu)$.

In the disordered spherulite model, the value of a expresses the correlation length of perturbation in the crystallite orientation, and the increase in a is interpreted as the ordering in the orientation of the crystallites. According to our interpretation above, $I_{iso}(q)$ originates from the uniform central part and is no longer expressed by $I_{iso}^{(0)}(q)$ of Eq. (2). At some stages, $25 < N < 50$ for $\beta_t = 10^\circ$ in the simulation, Eq. (2) can be a good approximation for $I_{iso}(q)$ as shown in Fig. 12. Since $I_{iso}(q)$ is, in principle, expressed in terms of the shape and the size of the uniform central part and decreases with q apart from the oscillation at high q, the ''correlation'' length a is regarded as the size of the uniform part, which grows with crystallization time in stages (i) and (ii). In the disordered spherulite model the spherulite radius R is given by $4.09/q_{max}$. In our interpretation the profile of $I_{4\text{-fold}}(q)$ and its peak position q_{max} depends on the size and the shape of the spherulite: the value of $1/q_{max}$ is approximately proportional to the size of spherulite in stage (ii) and $4.09/q_{max}$ gives the spherulite radius in stage (iii). The melt-grown axialites or hedrites will be a suitable system, and the Vv scattering experiments as well as the Hv scattering will give effective information in order to examine the above interpretation [15].

In summary, we have simulated the growth of a spherulite and calculated the Hv scattering intensity. The simulation results well reproduce the prominent features characterizing the Hv scattering intensity observed in the experiment. We have proposed an interpretation on the development of the Hv light scattering intensity in the spherulite formation process: at first the crystallites with uniform orientation grow and the spherulite mainly gives the isotropic intensity component. Then, the spherulite fans out by the overgrowth of the crystallites with spherical symmetry on the central uniform part and gives both the isotropic intensity component and the fourfold-symmetry intensity component. The spherulite that has grown sufficiently spherical mainly gives the ideal spherulite intensity.

Appendix

Let us consider a scattering body in which the polarizability is symmetrically distributed around a certain axis. When such scattering bodies are randomly oriented and spaced, we show that the resulting Hv light scattering is in general given by the sum of the intensity with the fourfold symmetry with regard to the azimuthal angle μ and the one independent of μ.

The scattered electric field E given by

$$E(\mathbf{q}) = C' \int (\mathbf{M}\cdot\hat{\mathbf{O}}) e^{-iq\cdot r} d\mathbf{r}, \tag{8}$$

$$\mathbf{M}(\mathbf{r}) = \alpha(\mathbf{r})\mathbf{E}_0, \tag{9}$$

where C' is a constant, $\mathbf{M}$, the induced dipole moment, $\mathbf{r}$, the position vector, $\boldsymbol{\alpha}(\mathbf{r})$, the polarizability tensor at position $\mathbf{r}$, $\mathbf{E}_0$, the electric filed of the incident beam, $\mathbf{q}$, the scattering vector and $\hat{\mathbf{O}}$ is the unit vector which is perpendicular to the propagation direction of the scattered ray and lies in a plane containing the polarization direction of the analyzer $\hat{\mathbf{A}}$ and perpendicular to the analyzer plane. In the following calculation of the Hv scattering intensity, the x-axis is defined as the polarization direction of the analyzer, the y-axis as that of the polarizer and the z-axis as the light propagation direction. When a scattering angle is small, $\hat{\mathbf{O}}$ can be approximated by $\hat{\mathbf{A}}$. In this case the amplitude of the Hv light scattering E_{Hv} is

$$E_{Hv}(\mathbf{q}) = C' \int \alpha_{xy}(\mathbf{r}) e^{-iq\cdot r} d\mathbf{r}, \tag{10}$$

where α_{xy} is the xy component of $\boldsymbol{\alpha}$ in the Cartesian basis representation.

We give an outline of the following calculation. (1) The distribution of the polarizability tensor which is rotationally symmetric around the z-axis is expanded by the spherical harmonic functions. (2) The scattering body is rotated and the orientation is specified by a set of Euler angles α, β and γ ($\gamma = 0$). (3) The scattering amplitude $E_{Hv}(\mathbf{q}; \alpha, \beta)$ is calculated for the rotated body. (4) The intensity $|E_{Hv}(\mathbf{q}; \alpha, \beta)|^2$ is averaged over α and β, and the μ dependence of the averaged intensity is examined.

A polarizability tensor is written as

$$\alpha = \frac{\alpha_{xx} + \alpha_{yy} + \alpha_{zz}}{3}\mathbf{I} + \mathbf{S}, \tag{11}$$

$$\mathbf{S}=\frac{1}{3}\begin{pmatrix} 2\alpha_{xx}-\alpha_{yy}-\alpha_{zz} & 3\alpha_{xy} & 3\alpha_{zx} \\ 3\alpha_{xy} & 2\alpha_{yy}-\alpha_{xx}-\alpha_{zz} & 3\alpha_{yz} \\ 3\alpha_{zx} & 3\alpha_{yz} & 2\alpha_{zz}-\alpha_{xx}-\alpha_{yy} \end{pmatrix} \tag{12}$$

where $\mathbf{I}$ is the unit tensor. A symmetric traceless tensor $\mathbf{S}$ is expressed by a linear combination of irreducible tensors of the second rank χ_{2i} ($i=-2,\ -1,\ 0,\ 1,\ 2$):

$$\mathbf{S}=\sum_i t_i(\mathbf{r})\chi_{2i}, \tag{13}$$

where $\boldsymbol{\chi}_{2i}$ in the Cartesian coordinate frame are

$$\chi_{20}=\frac{1}{3}\begin{pmatrix} -1 & 0 & 0 \\ 0 & -1 & 0 \\ 0 & 0 & 2 \end{pmatrix}, \tag{14}$$

$$\chi_{2\pm1}=\mp\frac{1}{\sqrt{6}}\begin{pmatrix} 0 & 0 & 1 \\ 0 & 0 & \pm i \\ 1 & \pm i & 0 \end{pmatrix}, \tag{15}$$

$$\chi_{2\pm2}=\frac{1}{\sqrt{6}}\begin{pmatrix} 1 & \pm i & 0 \\ \pm i & -1 & 0 \\ 0 & 0 & 0 \end{pmatrix}. \tag{16}$$

The xy component of $\boldsymbol{\alpha}$ can be expressed in terms of the coefficients t_i by

$$\alpha_{xy}(\mathbf{r})=\frac{i}{\sqrt{6}}(t_2(\mathbf{r})-t_{-2}(\mathbf{r})). \tag{17}$$

In a polar coordinate system (r, θ, φ), the angular distribution of the polarizability tensor is expressed by a linear combination of tensor spherical harmonics:

$$Y^{ls}_{jm}(\theta,\varphi)=\sum_{m',\sigma} C^{jm}_{lm's\sigma}Y_{lm'}(\theta,\varphi)\chi_{s\sigma}, \tag{18}$$

where s (=2) is a rank of irreducible tensor and Y_{lm}, is a spherical harmonic function. In the language of the wave functions with a spin quantum number s, j is a total angular momentum, m, its projection quantum number, l, an orbital angular momentum and $C^{jm}_{lm's\sigma}$, the Clebsch–Gordan coefficient.

When a tensor distribution of a scattering body has the rotational symmetry around the z-axis, $m=0$ holds. Then a distribution of symmetric traceless tensors is expressed by

$$\mathbf{S}(r,\theta,\varphi)=\sum_{jl} a_{jl}(r)Y^{l2}_{j0}(\theta,\varphi), \tag{19}$$

where $a_{jl}(r)$ is an r-dependent expansion coefficient.

Now, the scattering body is rotated by the Euler angles (α, β, γ). From the symmetry, we set $\gamma=0$. A rotated distribution $\mathbf{S}'$ is given by

$$\begin{aligned}\mathbf{S}'(r,\theta,\varphi)&=\widehat{\mathbf{D}}(\alpha,\beta,\gamma)\mathbf{S}(r,\theta,\varphi)\\&=\sum_{j,l} a_{j,l}(r)\sum_m Y^{l2}_{jm}(\theta,\varphi)D^{(j)}_{m0}(\alpha,\beta,0),\end{aligned} \tag{20}$$

where $\widehat{\mathbf{D}}(\alpha,\beta,\gamma)$ is the rotation operator and $D^{(j)}_{m'm}(\alpha,\beta,\gamma)$ is the Wigner D function, which is in the present case given by

$$D^{(j)}_{m0}(\alpha,\beta,\gamma)=\sqrt{\frac{4\pi}{2j+1}}\,Y^*_{jm}(\beta,\alpha). \tag{21}$$

Substituting Eqs. (18) and (21) into Eq. (20) gives the coefficients of $\boldsymbol{\chi}_{22}$ and $\boldsymbol{\chi}_{2-2}$ as

$$\begin{aligned}t_{\pm2}(\mathbf{r})=&\sum_{j=0}^{\infty}\sqrt{\frac{4\pi}{2j+1}}\sum_{l=|j-2|}^{j+2}a_{jl}(r)\\&\times\sum_{m=-j}^{j}C^{jm}_{lm\mp22\pm2}Y_{lm\mp2}(\theta,\varphi)Y^*_{jm}(\beta,\alpha).\end{aligned} \tag{22}$$

The scattering amplitude from the rotated distribution, $E_{\mathrm{Hv}}(\mathbf{q};\ \alpha,\ \beta)$, is given by Eqs. (10), (17) and (22) as

$$\begin{aligned}E_{H_v}(\mathbf{q};\alpha,\beta)=&\frac{i\sqrt{4\pi}C'}{\sqrt{6}}\sum_{j=0}^{\infty}\sum_{m=-j}^{j}\sum_{l=|j-2|}^{j+2}\frac{1}{\sqrt{2j+1}}Y^*_{jm}(\beta,\alpha)\\&\times\int a_{jl}(r)f_{jlm}(\theta,\varphi)\mathrm{e}^{-\mathrm{i}q\cdot r}\mathrm{d}r,\end{aligned} \tag{23}$$

where

$$f_{jlm}(\theta,\varphi)=C^{jm}_{lm-222}Y_{lm-2}(\theta,\varphi)-C^{jm}_{lm+22-2}Y_{lm+2}(\theta,\varphi).$$

The partial wave expansion,

$$\exp(-\mathrm{i}\mathbf{q}\cdot\mathbf{r})=4\pi\sum_{l=0}^{\infty}\sum_{m=-l}^{l}(-i)^l j_l(qr)Y_{lm}(\nu,\mu)Y^*_{lm}(\theta,\varphi), \tag{24}$$

where q, ν and μ are the polar coordinates in the reciprocal space and $j_l(qr)$ is the spherical Bessel function, and the orthogonality and the normalization relation of the spherical harmonics lead to

$$\begin{aligned}E_{H\mathrm{v}}(\mathbf{q};\alpha,\beta)=&\frac{8\pi^{3/2}iC'}{\sqrt{6}}\sum_{j=0}^{\infty}\sum_{m=-j}^{j}\sum_{l=|j-2|}^{j+2}\\&\times\frac{1}{\sqrt{2j+1}}Y^*_{jm}(\beta,\alpha)b_{jl}(q)\mathrm{g}_{jlm}(\nu,\mu),\end{aligned} \tag{25}$$

where

$$g_{jlm}(\nu,\mu)=C^{jm}_{lm-222}Y_{lm-2}(\nu,\mu)-C^{jm}_{lm+22-2}Y_{lm+2}(\nu,\mu)$$

and

$$b_{jl}(q)=(-i)^l\int a_{jl}(r)j_l(qr)r^2\mathrm{d}r.$$

The intensity from the scattering body $I_{\mathrm{Hv}}(\mathbf{q})$ is obtained by averaging over the Euler angles α and β:

$$I_{H_v}(\mathbf{q}) = \frac{1}{4\pi}\int |E_{H_v}(\mathbf{q};\alpha,\beta)|^2 \sin\beta \mathrm{d}\alpha\, \mathrm{d}\beta$$
$$= \frac{8\pi^2 C'^2}{3}\sum_{j=0}^{\infty}\sum_{m=-j}^{j}\sum_{l_1=|j-2|}^{j+2}\sum_{l_2=|j-2|}^{j+2} \times \frac{1}{2j+1} b_{jl_1}(q) b_{jl_2}(q)^* g_{jl_1m}(\nu,\mu) g_{jl_2m}(\nu,\mu)^*, \quad (26)$$

By using $Y_{lm}(\nu,\mu) = Y_{lm}(\nu,0)\mathrm{e}^{im\mu}$, we obtain

$$g_{jl_1m}(\nu,\mu) g_{jl_2m}(\nu,\mu)^* = h^+_{jl_1m}(\nu) h^+_{jl_2m}(\nu) + h^-_{jl_1m}(\nu) h^-_{jl_2m}(\nu) - h^+_{jl_1m}(\nu) h^-_{jl_2m}(\nu)\mathrm{e}^{-4i\mu} - h^-_{jl_1m}(\nu) h^+_{jl_2m}(\nu)\mathrm{e}^{4i\mu}, \quad (27)$$

where

$$h^{\pm}_{jlm}(\nu) \equiv C^{jm}_{lm\mp 22\pm 2} Y_{lm\mp 2}(\nu,0).$$

The intensity is therefore expressed by

$$I_{H_v}(\mathbf{q}) = \frac{8\pi^3 C^2}{3}\sum_{j=0}^{\infty}\sum_{m=-j}^{j}\sum_{l_1=|j-2|}^{j+2}\sum_{l_2=|j-2|}^{j+2}\frac{1}{2j+1} F_{jml_1l_2}(q,\nu,\mu) \quad (28)$$

where

$$F_{jml_1l_2}(q,\nu,\mu) = \mathrm{Re}\left[b_{jl_1}(q) b_{jl_2}(q)^*\right]\left(h^+_{jl_1m}(\nu) h^+_{jl_2m}(\nu) + h^-_{jl_1m}(\nu) h^-_{jl_2m}(\nu)\right) - \cos 4\mu\, \mathrm{Re}\left[b_{jl_1}(q) b_{jl_2}(q)^*\right]\left(h^+_{jl_1m}(\nu) h^-_{jl_2m}(\nu) + h^-_{jl_1m}(\nu) h^+_{jl_2m}(\nu)\right) - 2\sin 4\mu\, \mathrm{Im}\left[b_{jl_1}(q) b_{jl_2}(q)^*\right]\left(h^+_{jl_1m}(\nu) h^+_{jl_2m}(\nu) + h^-_{jl_1m}(\nu) h^-_{jl_2m}(\nu)\right). \quad (29)$$

Eqs. (28) and (29) show that the scattering intensity consists of a component independent of μ and another component with the fourfold symmetry regarding μ.

The component $(j, l) = (0, 2)$ in the summation of Eq. (19) expresses the polarizability distribution of the spherical symmetry, i.e., that of the ideal spherulite, and $(j, l) = (2, 0)$, the uniform distribution of polarizability. When the shape of the scattering body is a sphere, the component $(j, l) = (0, 2)$ in $|E_{\mathrm{Hv}}(\mathbf{q}; \alpha, \beta)|^2$ or in Eq. (28) is reduced to Eq. (1) of the ideal spherulite model with $C'^2 = C$ and $\Delta\alpha = \sqrt{1/4\pi}$, and the component $(j, l) = (2, 0)$ in Eq. (28) gives the isotropic scattering intensity independent of μ.

References

[1] Stein RS, Rhodes MB. J Appl Phys 1960;31:1873–84.
[2] Keijzers AEM, van Aartsen JJ, Prins W. J Am Chem Soc 1968;90:3107–13.
[3] Stein RS, Chu W. J Polym Sci A2 1970;8:1137–57.
[4] Hashimoto T, Stein RS. J Polym Sci A2 1971;9:1747–61.
[5] Yoon DY, Stein RS. J Polym Sci Polym Phys Ed 1974;12:763–84.
[6] Hashimoto M, Toda A, Miyaji H. Polymer 1992;33(5):909–13.
[7] Tahara D, Fukao K, Miyamoto Y. Polymer 2002;43:7461–5.
[8] Stein RS, Wilson PR. J Appl Phys 1962;33:1914–22.
[9] Stein RS, Stidham SN. J Appl Phys 1964;35(1):42–6.
[10] Hashimoto T, Prud'homme RE, Stein RS. J Polym Sci Polym Phys Ed 1973;11:709–36.
[11] Picot C, Stein RS, Motegi M, Kawai H. J Polym Sci A2 1970;8:2115–26.
[12] Champion JV, Killey A, Meeten GH. J Polym Sci Polym Phys Ed 1985;23(7):1467–76.
[13] Khoury K, Passaglia E. Treatise on solid state chemistry, vol. 3. New York: Plenum Press; 1976. p. 470.
[14] Vaughan AS, Bassett DC. Polymer 1988;29:1397–401.
[15] Hoffman A, Strobl G. Polymer 2003;44:5803–9.